

# Block Encoding of Sparse Matrices via Coherent Permutation

Abhishek Setty<sup>a,b,\*</sup>

<sup>a</sup>*Forschungszentrum Jülich, Institute of Quantum Control (PGI-8), D-52425 Jülich, Germany*

<sup>b</sup>*Institute for Theoretical Physics, University of Cologne, D-50937 Cologne, Germany*

---

## Abstract

Block encoding of sparse matrices underpins powerful quantum algorithms such as quantum singular value transformation, Hamiltonian simulation, and quantum linear solvers, but its efficient gate-level implementation for arbitrary sparse matrices remains a major challenge. We introduce a unified framework that overcomes the key obstacles of multi-controlled X gates overhead, amplitude reordering, and hardware connectivity, enabling efficient block encoding for arbitrary sparse matrices with explicit gate-level constructions. Central to our approach are a novel connection with combinatorial optimization, which enables systematic assignment of control qubits to achieve nearest-neighbor connectivity, and coherent permutation operators that preserve superposition while enabling amplitude reordering. We demonstrate our methods on structured sparse matrices, showing significant reductions in circuit depth and control overhead, thereby bridging the gap between theoretical formulations and practical circuit implementations for quantum algorithms.

*Keywords:* Block encoding, Quantum circuits, Quantum linear algebra, Combinatorial optimization

---

## Contents

<b>1</b>	<b>Introduction</b>	<b>1</b>
<b>2</b>	<b>Notations and Preprocessing</b>	<b>2</b>
<b>3</b>	<b>Block Encoding</b>	<b>3</b>
3.1	State Preparation Oracle . . . . .	4
3.2	Index Mapping Oracle . . . . .	4
<b>4</b>	<b>Composition of Multi-Controlled X Gates</b>	<b>5</b>
<b>5</b>	<b>Combinatorial Optimization Based Mapping of Basis States</b>	<b>6</b>
<b>6</b>	<b>Coherent Permutation Using Multi-Controlled X Gates</b>	<b>7</b>
<b>7</b>	<b>Optimized Index Mapping Oracle</b>	<b>8</b>
7.1	Shift . . . . .	8
7.2	Delete . . . . .	9
7.3	Insert . . . . .	10

<b>8</b>	<b>Complete Circuit</b>	<b>10</b>
<b>9</b>	<b>Applications</b>	<b>11</b>
9.1	Complex Tridiagonal Matrix . . . . .	11
9.2	Structured Real Matrix . . . . .	12
<b>10</b>	<b>Discussion</b>	<b>14</b>

## 1. Introduction

Block encoding has emerged as a central primitive in modern quantum algorithms, providing a systematic way to embed a matrix into a unitary operator and thereby enabling polynomial transformation of operators via Quantum Singular Value Transformation (QSVT) [1]. The idea was first used implicitly in early breakthroughs such as the Harrow-Hassidim-Lloyd (HHL) algorithm for solving linear systems of equations [2] and Hamiltonian simulation techniques [3–5], and was later formalized by Gilyén et al. [1]. Since then, block encoding has become indispensable in a wide range of domains including quantum linear algebra, optimization, machine learning and quantum chemistry [6–8]. Succinctly, block encoding is the process of embedding a given (possibly non-unitary) matrix  $A$

---

\*Corresponding author  
*Email address:* a.setty@fz-juelich.de (Abhishek Setty)

into a larger unitary operator  $U_A$  as,

$$U_A = \begin{pmatrix} A/\alpha & * \\ * & * \end{pmatrix}, \quad (1)$$

where  $\alpha$  is a subnormalization factor ensuring  $\|A/\alpha\|_2 \leq 1$ ,  $*$  denotes inconsequential blocks, and  $\|\cdot\|_2$  is the spectral norm. The factor  $\alpha$  and the presence of  $*$  blocks guarantee that a unitary  $U_A$  exists.

Understanding the importance of block encoding has led to substantial research efforts to optimize its construction for different matrix classes. For arbitrary dense matrices, resource requirements have been well studied [9, 10]. Approximate block encodings using single- and two-qubit gates have been developed through the FABLE method [11, 12], and subsequent improvements using demultiplexor operations have been proposed [13]. For sparse matrices, block encodings have typically been formulated in terms of black-box oracles [1], but these works often omit explicit circuit-level implementations. More detailed realizations have been provided for structured sparsity [14]. Since the subnormalization factor  $\alpha$  directly affects amplitude scaling in block encoding and consequently increases circuit depth in certain algorithms, recent works have sought to reduce it. Sünderhauf et al. [15] proposed schemes for matrices with arithmetic structure and PREP/UNPREP operators inspired by the Linear Combinations of Unitaries (LCU) method [5], while Yang et al. [16] introduced a dictionary-based protocol with improved subnormalization factor  $\sum_{p=0}^{s-1} |A_p|$ , where  $s$  is the number of unique diagonal elements in the matrix. Despite these advances, efficient, and fully explicit constructions for block encodings of sparse matrices remain largely unexplored.

In this work, we introduce a novel quantum data manipulation strategy within the block encoding framework, providing enhanced control over matrix-space reachability while significantly reducing reliance on multi-controlled X (MCX) gates. Our method generalizes naturally and advances efficient quantum circuit mapping and compilation [17–20], as well as reduces MCX control complexity [21–23]. We establish a novel connection between amplitude reordering by coherent permutation and combinatorial optimization, systematically assigning control qubits for MCX gates. This is particularly relevant for hardware with nearest-neighbor connectivity, where long-distance interactions increases noise and depth [24–26]. By optimizing con-

trol placement, our approach reduces circuit depth, improves hardware compatibility, and demonstrates practical benefits in block encoding of representative sparse matrices. We demonstrate our methods on structured sparse matrices, illustrating how theoretical advances translate into practical circuit implementations directly applicable to quantum algorithms.

## 2. Notations and Preprocessing

Assuming familiarity with standard conventions in the quantum computing literature, we establish following notations and conventions:

- For an  $N \times N$  matrix, the  $j^{\text{th}}$  column is denoted by  $|j\rangle$ , where  $j \in [0, N - 1]$ . Its binary representation is given by,

$$j \mapsto j_{n-1} \times 2^{n-1} + \cdots + j_0 \times 2^0 \mapsto |j_{n-1} \cdots j_1 j_0\rangle, \quad (2)$$

where  $j_k \in \{0, 1\}$ ,  $k \in [0, n - 1]$  and  $n$  is the number of qubits.

- Qubits in a circuit diagram are ordered increasingly from top to bottom, as illustrated for the three-qubit circuit  $U$  in Fig. 1a. The binary state  $|j_{n-1} \cdots j_1 j_0\rangle$  is mapped to the quantum register  $|q_0 q_1 \cdots q_{n-1}\rangle$ , such that the highest-index qubit  $|q_{n-1}\rangle$  corresponds to  $|j_0\rangle$ , and the lowest-index qubit  $|q_0\rangle$  corresponds to  $|j_{n-1}\rangle$  Fig. 1b.
- The Hamming distance [27, 28] between two binary strings  $\vec{x} = (x_0, x_1, \dots, x_{n-1})^T$  and  $\vec{y} = (y_0, y_1, \dots, y_{n-1})^T$ , where  $x_k, y_k \in \{0, 1\}$ , is defined as

$$D_H = |\vec{x} - \vec{y}| = \sum_{k=0}^{n-1} (x_k \oplus y_k), \quad (3)$$

where  $\oplus$  denotes the XOR operation. For instance,  $D_H(010, 001) = 2$ .

- For a computational basis state  $\vec{a}$  in binary representation Eq. (2), we denote by  $C_{\vec{a}}(U)$  the controlled unitary that applies  $U$  conditioned on the control register being in state  $\vec{a}$ .

To preprocess for block encoding, consider an  $l$ -sparse complex matrix  $A \in \mathbb{C}^{2^n \times 2^n}$ , where  $l$  denotes the maximum number of nonzero entries in any row or column. Each complex entry  $A_l$  is decomposed into its real and imaginary parts. The magnitudes

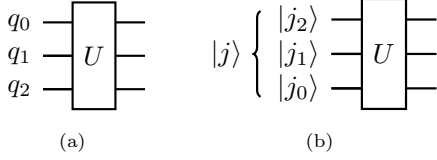


Figure 1: a Qubits of circuit  $U$  are numbered in increasing order from top to bottom. b The binary representation of an integer state  $|j\rangle$  is assigned to qubits in decreasing order from top to bottom.

of these nonzero components are then collected into a vector,

$$A_{\text{data}} = \begin{bmatrix} |\text{Re}(A_0)| \\ |\text{Im}(A_0)| \\ \vdots \\ |\text{Re}(A_{l-1})| \\ |\text{Im}(A_{l-1})| \end{bmatrix}_{s \times 1}, \quad (4)$$

where  $s \leq 2l$ , since zero-valued components are excluded. By construction,  $A_{\text{data}}$  contains only positive real values. To preserve the original sign (+/−) of the real and imaginary parts, we store them separately in a sign vector,

$$\text{sgn}(A_{\text{data}}) = \begin{bmatrix} \text{sgn}(\text{Re}(A_0)) \\ \text{sgn}(\text{Im}(A_0))i \\ \vdots \\ \text{sgn}(\text{Re}(A_{l-1})) \\ \text{sgn}(\text{Im}(A_{l-1}))i \end{bmatrix}_{s \times 1}, \quad (5)$$

where  $\text{sgn}(z) = \frac{z}{|z|}$  denotes the sign function, extended here to complex values, and  $i$  explicitly marks imaginary components.

### 3. Block Encoding

In this section, we extend the PREP/UNPREP-based block encoding scheme to handle complex sparse matrices and present a clear, intuitive framework for constructing the corresponding quantum circuits. Building on the dictionary-based block encoding protocol [16], we define the  $p^{\text{th}}$  data item  $A_p$  from  $A_{\text{data}}$ , where  $p \in [0, s-1]$ , such that each matrix element  $A_{ij}$  can be represented at row index  $i$  and column index  $j$ . The set of all column indices associated with  $A_p$  is denoted as  $S_c(p)$ . The corresponding row index is determined by  $i = c_p(j)$ , where  $c_p(j)$  is an injective function mapping column indices  $j$  to their respective row indices  $i$ .

Based on these definitions, the required quantum oracles are:

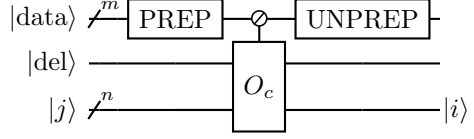


Figure 2: Circuit structure for block encoding of sparse matrices. A single qubit is represented by a plain wire (del qubit), while multiple qubits are depicted as a wire marked with a short slash, labeled with the number of qubits it contains ( $m$  for data qubits and  $n$  for matrix qubits  $|j\rangle$ ). The PREP and UNPREP blocks denote state-preparation operators. The multi-controlled  $O_c$  operator uses a control symbol drawn as a circle with a slash. The control values are determined by the binary representation in Eq. (2), following the qubit ordering convention shown in Fig. 1.

1. State Preparation: The oracles PREP and UNPREP embed the data vector  $A_{\text{data}} = [A_p]_{p=0}^{s-1}$  Eq. (4) and the sign vector  $\text{sgn}(A_{\text{data}}) = [\text{sgn}(A_{\text{data}})_p]_{p=0}^{s-1}$  Eq. (5) into the amplitudes of a quantum state.
2. Index Mapping: The oracle  $O_c$  implements the injective mapping  $c_p : j \mapsto c_p(j)$ , for  $p \in [0, s-1]$  and  $j \in S_c(p)$ .

With these oracles in place, the block encoding scheme is formulated as described in Theorem 1 [16].

**Theorem 1.** *Let  $A = \mathbb{C}^{2^n \times 2^n}$  be a matrix that has  $s$  data items, and  $m = \lceil \log_2 s \rceil$ . If there exists column oracle  $O_c$  such that*

$$O_c|p\rangle_{\text{data}}|0\rangle_{\text{del}}|j\rangle = \begin{cases} |p\rangle_{\text{data}}|0\rangle_{\text{del}}|c_p(j)\rangle, & \text{if } p \in [0, s-1] \text{ and } j \in S_c(p), \\ |p\rangle_{\text{data}}|0\rangle_{\text{del}}|j\rangle, & \text{if } p \in [s, 2^m - 1] \text{ or } j \notin S_c(p), \end{cases} \quad (6)$$

and two state preparation oracles PREP and UNPREP such that

$$\begin{aligned} \text{PREP}|0\rangle_{\text{data}}^{\otimes m} &= \frac{1}{\sqrt{\sum_{p=0}^{s-1} A_p}} \\ &\left( \sum_{p=0}^{s-1} \text{sgn}(A_{\text{data}})_p \sqrt{A_p} |p\rangle_{\text{data}} + \sum_{p=s}^{2^m-1} 0 |p\rangle_{\text{data}} \right), \end{aligned} \quad (7)$$

$$\begin{aligned} \text{UNPREP}^\dagger|0\rangle_{\text{data}}^{\otimes m} &= \frac{1}{\sqrt{\sum_{p=0}^{s-1} A_p}} \\ &\left( \sum_{p=0}^{s-1} \sqrt{A_p^*} |p\rangle_{\text{data}} + \sum_{p=s}^{2^m-1} 0 |p\rangle_{\text{data}} \right), \end{aligned} \quad (8)$$

where  $\sqrt{A_p}^*$  denotes the complex conjugate of  $\sqrt{A_p}$ , then the unitary,  $U_A = (\text{UNPREP} \otimes I_{2^{n+1}})O_c(\text{PREP} \otimes I_{2^{n+1}})$ , as shown in Fig. 2, can block encode  $A$  with the subnormalization  $\alpha = \sum_{p=0}^{s-1} A_p$ .

*Proof:* To recover the matrix from its block encoding, the flag qubits (i.e., the data and delete qubits) are initialized and postselected in the state  $|0\rangle$ . The matrix entries can then be reconstructed as  $\frac{A_{ij}}{\alpha} = \frac{\text{Re}(A_{ij})}{\alpha} + i\frac{\text{Im}(A_{ij})}{\alpha}$ . The procedure for combining the real and imaginary components will be detailed in Section 9.1. For the moment, we focus on the extraction of either the real or the imaginary part individually. This is achieved by initializing the bottom register with  $|j\rangle$  and postselecting (or measuring) the outcome  $|i\rangle$ , as follows:

$$\begin{aligned}
& \langle 0 |_{\text{data}}^{\otimes m} \langle 0 |_{\text{del}} \langle i | (\text{UNPREP} \otimes I_{2^{n+1}})O_c \\
& \quad (\text{PREP} \otimes I_{2^{n+1}}) | 0 \rangle_{\text{data}}^{\otimes m} | 0 \rangle_{\text{del}} | j \rangle \\
&= \frac{1}{\sqrt{\sum_{p'=0}^{s-1} A_{p'} \sum_{p=0}^{s-1} A_p}} \sum_{p',p=0}^{s-1} \langle p' |_{\text{data}} \langle 0 |_{\text{del}} \langle i | \\
& \quad \text{sgn}(A_{\text{data}})_p \sqrt{A_{p'} A_p} O_c | p \rangle_{\text{data}} | 0 \rangle_{\text{del}} | j \rangle \\
&= \frac{1}{\sqrt{\sum_{p'=0}^{s-1} A_{p'} \sum_{p=0}^{s-1} A_p}} \sum_{p',p=0}^{s-1} \langle p' |_{\text{data}} \langle i | \\
& \quad \text{sgn}(A_{\text{data}})_p \sqrt{A_{p'} A_p} \delta_{p,[0,s-1]} \delta_{j,S_c(p)} | p \rangle_{\text{data}} | c_p(j) \rangle \\
&= \frac{1}{\sqrt{\sum_{p'=0}^{s-1} A_{p'} \sum_{p=0}^{s-1} A_p}} \sum_{p',p=0}^{s-1} \\
& \quad \text{sgn}(A_{\text{data}})_p \sqrt{A_{p'} A_p} \delta_{p,[0,s-1]} \delta_{j,S_c(p)} \delta_{p,p'} \delta_{i,c_p(j)} \\
&= \frac{1}{\sum_{p=0}^{s-1} A_p} \text{sgn}(A_{\text{data}})_p A_p,
\end{aligned}$$

where  $\delta$  denotes a kronecker delta function  $\delta_{ij} = 1$  if  $i = j$ , else 0.

Next, we provide the gate-level implementation of the quantum operations described earlier.

### 3.1. State Preparation Oracle

The task of state preparation oracles PREP/UNPREP is to embed the data into amplitudes of a quantum state. Möttönen et al. [29, 30] introduced a state preparation method based on uniformly controlled rotation gates, which can be decomposed into either multi-controlled rotations or sequences of single- and two-qubit gates. This construction leverages classical preprocessing (e.g., Gray code ordering) to compute

the required rotation angles efficiently. Later, Iten et al. [31] proposed a hardware-oriented approach that decomposes arbitrary isometries into single-qubit and CNOT gates, thereby reducing the CNOT count in practice. Both methods are exact, require no ancilla qubits, but generally scale exponentially in gate count and depth for arbitrary state preparation. More recent work has explored depth-optimized schemes [32], achieving circuit depths of  $\mathcal{O}(m)$  for an  $m$ -qubit state or  $\mathcal{O}(\log(ms))$  for  $s$ -sparse states. These improvements, however, often come at the cost of introducing additional ancilla qubits, which in some cases can scale exponentially with the problem size.

### 3.2. Index Mapping Oracle

Without the index mapping oracle  $O_c$  in Fig. 2, the block-encoded matrix reduces to a diagonal form,

$$\begin{bmatrix} \eta & & \\ & \ddots & \\ & & \eta \end{bmatrix} \text{ where } \eta = \frac{\sum_{p=0}^{s-1} \text{sgn}(A_{\text{data}})_p A_p}{\sum_{p=0}^{s-1} A_p}. \quad (9)$$

The role of the oracle  $O_c$  is to redistribute these values to their target positions within the matrix. This process involves two main steps: shifting [14] and deletion [15].

For instance, consider the data vector  $A_{\text{data}} = [a, b, c, d]^T$  and the block encoding circuit without the index mapping oracle  $O_c$  in Fig. 2. Using three matrix qubits  $|j\rangle$  for an  $8 \times 8$  matrix, the resulting block encoded matrix is diagonal, as in Eq. (9). Suppose these data items are intended to be shifted left or right by  $(1, 2, 3, 4)$  columns, respectively. The resulting matrix representations after shifting are denoted by Eq. (10) and Eq. (11), where the subscript indicates the data item and the number of columns shifted, and the superscript  $r$  corresponds to the row index ( $r \in [0, 2^n - 1]$ ) for each element  $L_{a1}^r$  or  $R_{a1}^r$ .

$$L = \begin{bmatrix} 0 & 0 & 0 & 0 & L_{d4}^0 & L_{c3}^0 & L_{b2}^0 & L_{a1}^0 \\ L_{a1}^1 & 0 & 0 & 0 & 0 & L_{d4}^1 & L_{c3}^1 & L_{b2}^1 \\ L_{b2}^2 & L_{a1}^2 & 0 & 0 & 0 & 0 & L_{d4}^2 & L_{c3}^2 \\ L_{c3}^3 & L_{b2}^3 & L_{a1}^3 & 0 & 0 & 0 & 0 & L_{d4}^3 \\ L_{d4}^4 & L_{c3}^4 & L_{b2}^4 & L_{a1}^4 & 0 & 0 & 0 & 0 \\ 0 & L_{d4}^5 & L_{c3}^5 & L_{b2}^5 & L_{a1}^5 & 0 & 0 & 0 \\ 0 & 0 & L_{d4}^6 & L_{c3}^6 & L_{b2}^6 & L_{a1}^6 & 0 & 0 \\ 0 & 0 & 0 & L_{d4}^7 & L_{c3}^7 & L_{b2}^7 & L_{a1}^7 & 0 \end{bmatrix} \quad (10)$$

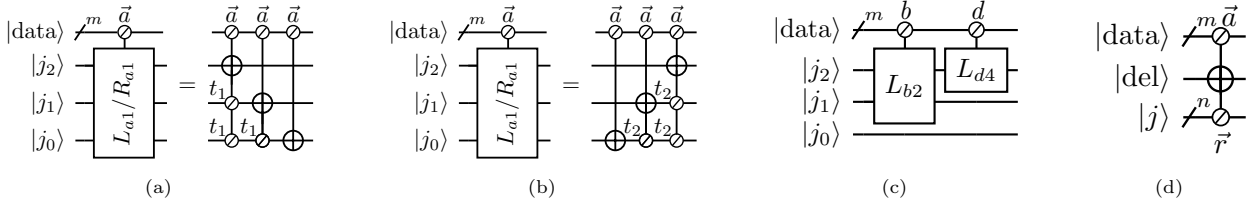


Figure 3: a Circuit illustration of a data item (a) from  $m$  data qubits being selected and shifted by one column in an  $8 \times 8$  matrix formed by three matrix qubits ( $|j\rangle$ ). The control values for the left shift ( $L_{a1}$ ) are  $t_1 = 1$ , while for the right shift ( $R_{a1}$ ), they are  $t_1 = 0$ . The binary vector  $\vec{a}$  (as defined in Eq. (2)) is placed above the circle with a slash to indicate the control values according to the qubit ordering in Fig. 1. b Alternative circuit for shifting the same data item (a), where the left shift ( $L_{a1}$ ) has  $t_2 = 0$  and the right shift ( $R_{a1}$ ) has  $t_2 = 1$ . c Circuit representation of shifting data item (b) by two columns ( $L_{b2}$ ) and data item (d) by four columns ( $L_{d4}$ ) to the left in the same  $8 \times 8$  matrix. d A data item (a) in the  $r^{\text{th}}$  row ( $L_a^r/R_a^r$ ) can be deleted by applying the control ( $\vec{a}$ ) on the data qubits ( $|\text{data}\rangle$ ) and ( $\vec{r}$ ) on the matrix qubits ( $|j\rangle$ ), followed by a NOT operation on the delete qubit ( $|\text{del}\rangle$ ).

$$R = \begin{bmatrix} 0 & R_{a1}^0 & R_{b2}^0 & R_{c3}^0 & R_{d4}^0 & 0 & 0 & 0 \\ 0 & 0 & R_{a1}^1 & R_{b2}^1 & R_{c3}^1 & R_{d4}^1 & 0 & 0 \\ 0 & 0 & 0 & R_{a1}^2 & R_{b2}^2 & R_{c3}^2 & R_{d4}^2 & 0 \\ 0 & 0 & 0 & 0 & R_{a1}^3 & R_{b2}^3 & R_{c3}^3 & R_{d4}^3 \\ R_{d4}^4 & 0 & 0 & 0 & 0 & R_{a1}^4 & R_{b2}^4 & R_{c3}^4 \\ R_{c3}^5 & R_{d4}^5 & 0 & 0 & 0 & 0 & R_{a1}^5 & R_{b2}^5 \\ R_{b2}^6 & R_{c3}^6 & R_{d4}^6 & 0 & 0 & 0 & 0 & R_{a1}^6 \\ R_{a1}^7 & R_{b2}^7 & R_{c3}^7 & R_{d4}^7 & 0 & 0 & 0 & 0 \end{bmatrix} \quad (11)$$

To shift a data item (a) left or right by one column, the circuits can be constructed as shown in Figs. 3a and 3b, where the control values on the  $m$  data qubits are determined by the binary representation of the data item ( $\vec{a}$ ). The control values  $t_1$  or  $t_2$  are selected depending on whether the shift is to the left or right.

For shifting a data item (b) by two columns, the pattern of MCX gates as in Figs. 3a and 3b are applied up to the  $|j_1\rangle$  qubit, while leaving  $|j_0\rangle$  idle, as illustrated in Fig. 3c. Similarly, for a data item (d) shifted by four columns, the pattern of MCX gates are applied up to the  $|j_2\rangle$  qubit, while leaving  $|j_1\rangle, |j_0\rangle$  idle (see Fig. 3c). In general, shifts are performed in the powers of 2. For shifting of data item (c) by three columns, the operation is decomposed as a combination of shifts by one and two columns:  $L_{c3} = L_{c2}L_{c1}$ . In this way, any arbitrary shift can be implemented as a combination of powers of 2. For complex-valued data Eqs. (4) and (5), the real and imaginary components must be shifted by the same number of columns to ensure correct addition in the encoded matrix.

The next key step in the index mapping oracle is the deletion of data items in the encoded matrix, since, by default, each data item appears once in

every row and column. For example, a data item ( $\vec{a}$ ) in row ( $\vec{r}$ ) can be deleted as illustrated in Fig. 3d.

#### 4. Composition of Multi-Controlled X Gates

Index mapping oracle proposed in this work relies on MCX gates, however, their hardware implementation limits scalability. In this section, we explore the simplification of MCX gates with certain structure.

Consider successive shift operators applied to two data items  $a$  and  $b$ , either left or right by one column in the block-encoded matrix formed by three matrix qubits  $|j\rangle$  (refer Fig. 3a). Since the control conditions being defined on orthogonal computational basis states  $\vec{a}$  and  $\vec{b}$  ( $\vec{a} \neq \vec{b}$ ) of the data qubits, the corresponding MCX gates act on mutually orthogonal subspaces of the Hilbert space. This orthogonality implies that the projectors  $|\vec{a}\rangle\langle\vec{a}|$  and  $|\vec{b}\rangle\langle\vec{b}|$  commute. Consequently, the MCX gates can be grouped as shown in Fig. 4, leading to various compositions ( $\prod$  MCX) with shared control and target qubits. Similarly, successive deletion operations of a specific data item across multiple rows also give rise to compositions of MCX gates (refer Fig. 3d). A recurring pattern in both types of operations is the composition of MCX gates acting on the same sets of control and target qubits.

Let all possible  $P$ -bit binary strings be given by set  $S_1 = \{a^j\}_{j=0}^{2^P-1}$ . Let the indices  $I = [P-1, \dots, 0]$ ,  $|I| = P$  according to the order Eq. (2) (refer Fig. 1). Note that,  $|\cdot|$  may refer to the cardinality of a set or the length of a vector, depending on context. Then each binary string is written as  $a^j = [a_i^j], i \in I$ , where  $a_i^j \in \{0, 1\}$  is the  $i$ -th bit of  $a^j$ . Consider a composition of  $2^n$  ( $1 \leq n < P$ ) MCX

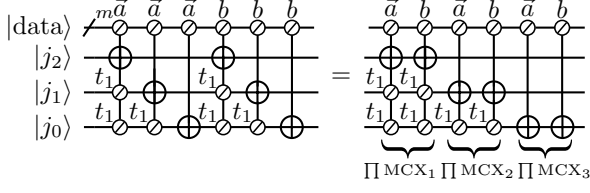


Figure 4: Shifting data items  $(a, b)$  towards left ( $t_1 = 1$ )/right ( $t_1 = 0$ ) in block encoded matrix formed by three matrix qubits  $|j\rangle$ . The MCX gates are grouped together resulting in three compositions  $\prod \text{MCX}$ .

gates as  $\prod_{j=0}^{2^n-1} \text{MCX}(a^j, t)$  acting on  $P + 1$  qubits

( $P > 1$ ), where the target  $X_{|t\rangle}^j$  is on qubit  $t \in [0, P]$  and control  $C$  is on remaining  $P$  qubits. Let the control of  $2^n$  computational basis states ( $|a^j\rangle$ ) are given by set of binary strings  $S_2 = \{a^j\}_{j=0}^{2^n-1}$ , where  $S_2 \subset S_1$ . Using these notations, we formulate the simplification of composition of MCX gates as in theorem below.

**Theorem 2.** *Given a composition of MCX gates  $\prod_{j=0}^{2^n-1} \text{MCX}(a^j, t)$ , and control set  $S_2 = \{a^j\}$ , if there exist fixed bits given by indices  $F \subset I, |F| = P - n$ , where  $a_i^j = a_i^k \forall i \in F, \forall j, k \in \{0, \dots, 2^n - 1\}$  such that  $\max_{j \neq k} D_H(a^j, a^k) = n$ , then  $\prod_{j=0}^{2^n-1} \text{MCX}(a^j, t) = \prod_j C_{|a^j\rangle} X_{|t\rangle} = \text{MCX}(\tilde{a}, t) = C_{|\tilde{a}\rangle} X_{|t\rangle}$ , where  $\tilde{a} = [\tilde{a}_i], i \in F$ .*

*Proof:* Consider each MCX gate is written as,

$$C_{|a^j\rangle} X_{|t\rangle} = |a^j\rangle\langle a^j| \otimes X_{|t\rangle} + (I - |a^j\rangle\langle a^j|) \otimes I_{|t\rangle},$$

where the identity operator  $I$  has dimension corresponding to the number of qubits it acts on. Let  $|\tilde{a}\rangle$  denote the state with fixed bits  $\{\tilde{a}_i\}, i \in F$  and  $|a'^j\rangle$  denote the state with varying bits  $\{a'_i\}, i \in I \setminus F$ . For the sake of derivation, we reorder the qubits so that the fixed indices are grouped together, allowing us to rewrite the control state as,

$$|a^j\rangle\langle a^j| = |\tilde{a}\rangle\langle \tilde{a}| \otimes |a'^j\rangle\langle a'^j|.$$

Then the product of MCX gates can be written as,

$$\prod_j C_{|a^j\rangle} X_{|t\rangle} = \prod_j [|\tilde{a}\rangle\langle \tilde{a}| \otimes |a'^j\rangle\langle a'^j| \otimes X_{|t\rangle} + (I - |\tilde{a}\rangle\langle \tilde{a}| \otimes |a'^j\rangle\langle a'^j|) \otimes I_{|t\rangle}].$$

In this product expansion, due to orthogonality  $\langle a'^j | a'^k \rangle = \delta_{jk}$ , the cross-terms get eliminated resulting in the summation as,

$$\prod_j C_{|a^j\rangle} X_{|t\rangle} = \sum_j (|\tilde{a}\rangle\langle \tilde{a}| \otimes |a'^j\rangle\langle a'^j| \otimes X_{|t\rangle} + (I - |\tilde{a}\rangle\langle \tilde{a}|) \otimes |a'^j\rangle\langle a'^j| \otimes I_{|t\rangle}),$$

where  $\sum_j |a'^j\rangle\langle a'^j| = I$ , since the summation of projectors over an orthonormal basis forms the identity operator. Therefore, the above expression can be further simplified to,

$$\prod_j C_{|a^j\rangle} X_{|t\rangle} = |\tilde{a}\rangle\langle \tilde{a}| \otimes I \otimes X_{|t\rangle} + (I - |\tilde{a}\rangle\langle \tilde{a}|) \otimes I \otimes I_{|t\rangle} = C_{|\tilde{a}\rangle} X_{|t\rangle}.$$

Note that, when  $n = P$ , then  $\prod_j C_{|a^j\rangle} X_{|t\rangle} = X_{|t\rangle}$  is simply a Pauli  $X$  gate on target qubit  $|t\rangle$ .

## 5. Combinatorial Optimization Based Mapping of Basis States

In this section, we generalize the simplification of composition of MCX gates whose control and target qubits are the same, but whose control sets do not satisfy the constraints in Theorem 2. To address this, we introduce a permutation of amplitudes among the basis states, after which the control states satisfy the required constraints. In other words, we map the set of desired control basis states from an unsuitable pattern to a suitable one.

Let all possible  $P$ -bit binary strings is given by set  $S_1 = \{a^j\}_{j=0}^{2^P-1}$ . Let an arbitrary set of  $P$ -bit binary strings is given by  $S_2 = \{a^j\}_{j=0}^{2^n-1}, (1 \leq n < P), S_2 \subset S_1$ . For a set of fixed indices  $F \subset I, |F| = P - n$ , we define a set  $S_3 = \{b^j\}_{j=0}^{2^n-1}, S_3 \subset S_1$ , where  $|b^j| = P, b_i^j = b_i^k \forall i \in F, \forall j, k \in \{0, \dots, 2^n - 1\}$  and  $\max_{j \neq k} D_H(b^j, b^k) = n$ . Note that, here  $|\cdot|$  denote the number of bits in the binary string. The objective is to find a set  $S_3$  that satisfies the structural constraints imposed by  $F$  while minimizing the total Hamming distance between  $S_2$  and  $S_3$ . We propose a solution to this problem in Theorem 3, where it is formulated as a special case of a combinatorial optimization problem with a bijective constraint.

**Theorem 3.** *Given an arbitrary set of binary strings  $S_2$  and a set of fixed indices  $F \subset I, |F| = P - n$ , there exist at least one set  $S_3$  and at least one bijection  $\phi : S_2 \mapsto S_3$  that minimizes  $\sum_{x \in S_2} D_H(x, \phi(x))$ .*

*Proof:* Consider the set  $S_2 = \{a^j\}_{j=0}^{2^n-1}$ . Let the most common bit pattern among the set of fixed indices  $F$  be

$$\tilde{a} = \underset{j \in [0, \dots, 2^n-1]}{\text{mode}} (\{a_i^j\}_{i \in F}), \quad (12)$$

where *mode* returns the most frequent sub-string. In case of ties, there will be more than one  $S_3$ , where one may impose tie-breaking rules or compute the total minimized Hamming cost for each possible  $S_3$  and select the one yielding the minimum.

For the sake of derivation, we consider one set and construct  $S_3 = \{b^j\}_{j=0}^{2^n-1}$ , where  $b_i^j = \tilde{a}_i, \forall i \in F, \forall j \in [0, \dots, 2^n-1]$  and  $\max_{j, k \in [0, \dots, 2^n-1]} D_H(b^j, b^k) = n$ . Now we exclude the common strings in  $S_2$  and  $S_3$  as  $S'_2 = S_2 \setminus S_3, S'_3 = S_3 \setminus S_2$ , as they are already matching.

Define the cost matrix  $C$  where each element  $C_{jk}$  is the Hamming distance between strings in sets  $S'_2, S'_3$  given as,

$$C_{jk} = D_H(a^j, b^k), j \in [0, \dots, |S'_2|-1], k \in [0, \dots, |S'_3|-1], \quad (13)$$

where  $|\cdot|$  denote the cardinality of the set and  $|S'_2| = |S'_3|$ .

The problem of finding  $\phi$  can be formulated as the binary integer linear program (ILP),

$$\begin{aligned} & \min \sum_j \sum_k C_{jk} x_{jk}, \\ & \text{s.t. } \sum_k x_{jk} = 1, \forall j, \\ & \quad \sum_j x_{jk} = 1, \forall k, \\ & \quad x_{jk} \in \{0, 1\}, \forall j, k, \end{aligned} \quad (14)$$

where  $x_{jk} = 1$  indicates  $\phi(a^j) = b^k$ .

This is a *linear assignment problem* in its purest form and can be solved in  $O(|S'_2|^3)$  time using the Hungarian method [33–36]. The existence of an optimal solution to this problem establishes the existence of the required bijection  $\phi$ . Choosing the most common bit pattern  $\tilde{a}$  Eq. (12) maximizes the overlap  $|S_2 \cap S_3|$  and therefore minimizes the residual set size  $|S'_2|$ , which reduces the scale of the subsequent assignment problem and is advantageous for optimization.

In general, there may be multiple optimal bijections  $\phi$  that achieve the same minimum total cost. One may then impose deterministic tie-breaking rules, such as lexicographic ordering of index pairs

$(j, k)$ . Alternatively, uniqueness can be enforced by perturbing the cost matrix, e.g. replacing each entry  $C_{jk}$  with  $C_{jk} + \epsilon r_{jk}$ , where  $\epsilon > 0$  is arbitrarily small and  $\{r_{jk}\}$  are distinct perturbations (random or deterministic). With such an  $\epsilon$ -perturbation, the minimizer is unique with probability one and corresponds to a canonical tie-broken solution of the original unperturbed problem [35, 37, 38].

## 6. Coherent Permutation Using Multi-Controlled X Gates

In this section, we introduce coherent permutation of amplitudes among basis states using MCX gates, where *coherent* denotes unitary (reversible) reordering that preserves superposition and relative phases without measuring or collapsing the quantum state.

Consider any  $P$ -qubit quantum state,  $|\psi\rangle = \sum_{i=0}^{2^P-1} \psi_i |i\rangle$  with  $2^P$  amplitudes corresponding to the computational basis states. The binary indices are  $I = [P-1, \dots, 0]$  according to Eq. (2) (refer to Fig. 1). Let a basis state  $|a\rangle$  be represented by the binary string  $\{a_j\}, j \in I$ . Then two amplitudes can be unitarily swapped among their basis states using A\_SWAP, as defined in Definition 6.1.

**Definition 6.1.** A\_SWAP( $a, b$ ): Consider two amplitudes with basis states  $\psi_a |a\rangle$  and  $\psi_b |b\rangle$ , where  $a$  and  $b$  only differ in the  $t$ -th qubit, i.e.,  $a_j = b_j \forall j \in I \setminus t$  and  $a_t \oplus b_t = 1, t \in I$ . Define the common control string  $c$  as  $c_j = a_j = b_j, \forall j \in I \setminus t$ . Then the two amplitudes can be swapped as,

$$\psi_a |a\rangle, \psi_b |b\rangle \mapsto \psi_b |a\rangle, \psi_a |b\rangle,$$

by applying the gate  $C_{|c\rangle} X_{|t\rangle}$ .

Note that after swapping, the order of amplitudes among the basis states is updated. We now consider the permutation of amplitudes (Definition 6.2), where amplitudes in the subset of basis states  $S_2 \subset S_1$  are permuted into another subset  $S_3 \subset S_1$  according to a bijection  $\phi : S_2 \mapsto S_3$ , which is obtained via the optimization procedure described in Theorem 3.

**Definition 6.2.** A\_PERMUTE( $S_2, S_3$ ): Let  $\tilde{S}_2 = \tilde{S}_3 = S_2 \cap S_3$  denote the set of basis states whose amplitudes are already in their target positions. Define the remaining states to be mapped as  $S'_2 = S_2 \setminus S_3$

and  $S'_3 = S_3 \setminus S_2$ . The permutation of the remaining amplitudes is then carried out as follows,

$$A\_PERMUTE = \begin{cases} A\_SWAP(a^j, b^j), a^j \in S'_2, b^j \in S_1 \setminus \tilde{S}_3 \\ \text{if } D_H(a^j, b^j) > 1, a^j \in S'_2, b^j \in S'_3 \\ A\_SWAP(a^j, b^j), a^j \in S'_2, b^j \in \tilde{S}_3 \\ \text{if } D_H(a^j, b^j) = 1, a^j \in S'_2, b^j \in S'_3 \end{cases} . \quad (15)$$

Note that after every A\_SWAP, all the sets are updated in the Definition 6.2. The A\_PERMUTE operator again consists of composition of MCX gates Section 4, but the control and target qubits can be on different qubits.

As seen in Theorem 2, a composition of MCX gates can be simplified into a single MCX gate when the control states satisfy certain constraints. Now we consider the inverse question: how a single MCX gate can be expressed as a composition of MCX gates, as formalized in the following theorem.

**Theorem 4.** For a given control state  $|\tilde{a}\rangle$  where binary string is  $\{\tilde{a}_i\}, i \in F \subset I$ , there exists a set of control states  $S_2 = \{a^j\}$  where  $|S_2| = 2^n, a_i^j = a_i^k \forall i \in F, \forall j, k \in \{0, \dots, 2^n - 1\}$  and  $\max_{j \neq k} D_H(a^j, a^k) = n$ , such that,  $MCX(\tilde{a}, t) =$

$$C_{|\tilde{a}\rangle} X_{|t\rangle} = \prod_{j=0}^{2^n-1} MCX(a^j, t) = \prod_j C_{|a^j\rangle} X_{|t\rangle} .$$

The proof of this theorem follows by reversing the steps of Theorem 2. In other words, the action of a single MCX gate  $MCX(\tilde{a}, t)$  is identical to performing A\_SWAP on all pairs of amplitudes whose control states belong to  $S_2$ . For example, consider three qubits  $(j_2, j_1, j_0)$  (refer Fig. 1) with quantum state vector  $[\psi_i]_{i=0}^7$ . A CNOT gate applied on two qubits according to Theorem 4 leads to the composition  $C_{(X1)} X_{j_0} = C_{(01)} X_{j_0} C_{(11)} X_{j_0}$ , which results in the following swapped amplitudes:

$$C_{(X1)} X_{j_0} = \begin{bmatrix} \psi_0 \\ \psi_1 \\ \psi_2 \\ \psi_3 \\ \psi_4 \\ \psi_5 \\ \psi_6 \\ \psi_7 \end{bmatrix} = \begin{bmatrix} \psi_0 \\ \psi_1 \\ \psi_3 \\ \psi_2 \\ \psi_4 \\ \psi_5 \\ \psi_7 \\ \psi_6 \end{bmatrix} . \quad (16)$$

Note that one can also use SWAP gate for permuting the amplitudes when it is available as native gate in the hardware; otherwise, the SWAP gate is indeed decomposed into three CNOT gates.

## 7. Optimized Index Mapping Oracle

In this section, we discuss the optimized operations in index mapping oracle (refer Section 3.2) and illustrate the theory proposed in Sections 4 to 6 through several examples in block encoding of sparse matrices, covering variety of applications.

### 7.1. Shift

We have seen the shift operator in Figs. 3a to 3c for a single data item. We now extend this to perform a combined operation on multiple data items. Consider a set of data items that are to be shifted left ( $L$ ) or right ( $R$ ) by the same number of columns. Let the set of basis states corresponding to these data items be  $S_2$ , with  $|S_2| = 2^n$ . If  $S_2$  satisfies the constraint in Theorem 2, then the individual shifts can be combined into a single shift operation.

Otherwise, one can choose a set of fixed indices  $F \subset I$  and generate  $S_3$  via an optimization-based mapping  $\phi : S_2 \mapsto S_3$  (refer Section 5). The choice of fixed indices  $F$  determines the qubits on which the MCX gates are applied. For instance, selecting the rightmost bits in the binary string as  $F = [P-n, \dots, 0]$  results in nearest-neighbor MCX gates between data and matrix qubits as illustrated in Example 7.2. Let  $A\_PERMUTE_R$  denote the permuting operator defined in Definition 6.2 corresponding to  $\phi : S_2 \mapsto S_3$  with right-ended fixed indices. Then, the circuit for the combined shift operation is shown in Fig. 5a. After shifting, the amplitudes are rearranged back to retain the original order, avoiding confusion in subsequent operations. Similarly, one may choose an arbitrary  $F$  according to the hardware qubit connectivity.

We now present some examples for intuitive understanding. Consider an  $8 \times 8$  matrix as in Eq. (10), with three matrix qubits ( $|j\rangle$ ) and two data qubits ( $|data\rangle$ ), representing four data items  $\{a, b, c, d\}$  in basis states  $(00, 01, 10, 11)$ , respectively.

**Example 7.1.** The data items  $\{a, b\}$  are to be shifted left by one column using the operators  $(L_{a1}, L_{b1})$ , corresponding to a many-to-one mapping.

*Solution:* When shifted individually, the operators can be given as  $L_{a1} = C_{(00)}(L_1), L_{b1} = C_{(01)}(L_1)$ . The composition of the two shift operations can be rearranged as shown in Fig. 4. The control states  $S_2 = \{00, 01\}$  satisfy the constraint in

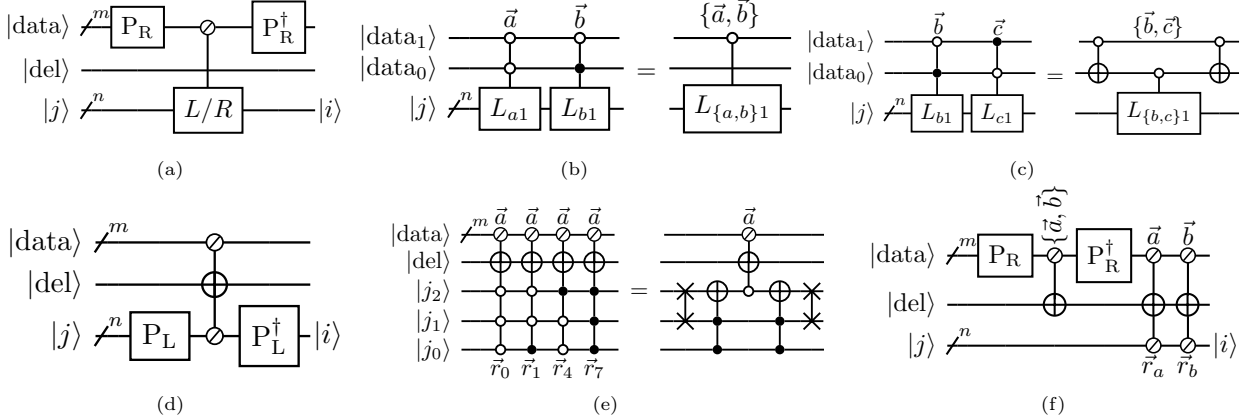


Figure 5: a Circuit representation of combined shift operation with right-ended permutation of amplitudes  $A_{\text{PERMUTE}_R}$  (represented by  $P_R$ ). b Circuit for Example 7.1, showing the combined left shift of data items  $(a, b)$  by one column. c Circuit for Example 7.2, illustrating permutation of amplitudes and left shift of data items  $(b, c)$  by one column. d Circuit representation of combined deletion with left-ended permutation of rows  $A_{\text{PERMUTE}_L}$  (represented by  $P_L$ ). e Circuit for Example 7.3, showing deletion of data item  $(a)$  in rows  $(0, 1, 4, 7)$ . f Circuit for Example 7.4, illustrating the insertion of data items  $(a, b)$  in rows  $(r_a, r_b)$ , respectively, along with  $P_R$ .

Theorem 2, allowing a combined operation. Therefore, the combined shift is

$$L_{\{a,b\}1} = L_{a1}L_{b1} = C_{(0X)}(L_1), \quad (17)$$

where  $X$  in the binary string indicates that no control gate is present on that qubit. The corresponding circuit representation is shown in Fig. 5b.

**Example 7.2.** The data items  $\{b, c\}$  are to be shifted left by one column using the operators  $(L_{b1}, L_{c1})$ , corresponding to a many-to-one mapping.

*Solution:* The control states  $S_2 = \{01, 10\}$  does not satisfy the constraint in Theorem 2, so permutation is required, as illustrated in Fig. 5a. We apply  $A_{\text{PERMUTE}_R}$ , where the amplitudes of  $a(00), b(01)$  are swapped using a CNOT (control value is 0) gate, as shown in Fig. 5c. After this permutation, the combined shift operator can be applied:

$$L_{\{b,c\}1} = L_{b1}L_{c1} = C_{X0}(L_1). \quad (18)$$

This example illustrates that right-ended permutation results in nearest-neighbor MCX gates.

**Example 7.3.** Assume a data vector  $A_{\text{data}}$  of 7 values, prepared in a state vector padded with 0:  $A_{\text{data}} = [a, b, c, d, e, f, g, 0]^T$ . The task is to shift the data items  $\{a, f, g\}$  left by one column.

*Solution:* According to Theorem 2, a combined operation is only possible when the number of shift operations is a power of two ( $2^n$ ). Since the task involves three data items, a naive approach would be to apply  $L_{\{a,f\}1}L_{g1}$ . Alternatively, one can exploit the 0 in the data vector and perform a combined shift on four data items  $\{a, f, g, 0\}$ , as shifting 0 does not affect the block-encoded matrix Eq. (9). The combined operation for these basis states requires permutation, as illustrated in Fig. 5a.

Note that shifting a single data item left and then right results in the identity operation, i.e.,  $L_{a1}R_{a1} = I$  (refer Figs. 3a and 3b). This property can be exploited when applying combined operations to simplify MCX gates.

## 7.2. Delete

We have seen how a single data item can be deleted in a specific row Fig. 3d. In this section, we generalize this to deletion in multiple rows. Consecutive delete operations of a single data item across multiple rows result in a composition of MCX gates with control and target on the same qubits. When the control states of such a composition satisfy the constraint in Theorem 2, they can be combined into a single MCX gate.

Otherwise, one can choose a set of fixed indices  $F \subset I$  and generate  $S_3$  via an optimization-based mapping  $\phi : S_2 \mapsto S_3$  (refer Section 5). For example, by selecting the left-end bits in the binary strings as fixed indices,  $F = [P-1, \dots, P-n]$ , the

control qubits in the MCX gates become nearest-neighbors between data and matrix qubits as illustrated in Example 7.4. Let  $A_{\text{PERMUTE}_L}$  denote the permuting operator (refer Definition 6.2) corresponding to  $\phi : S_2 \mapsto S_3$  with left-end fixed indices. The circuit for the combined delete operation is shown in Fig. 5d.

**Example 7.4.** *The data item  $a$  is to be deleted in rows  $\{0, 1, 4, 7\}$  using the operators  $(D_a^0, D_a^1, D_a^4, D_a^7)$ , corresponding to a one-to-many mapping.*

*Solution:* The set of control states  $S_2 = \{0, 1, 4, 7\}$  does not satisfy the constraint in Theorem 2, and therefore a permutation is required, as illustrated in Fig. 5d. Following Theorem 3, the bijection  $\phi : S_2 \mapsto S_3$  is obtained using the linear sum assignment algorithm [39], yielding  $\phi : S_2 = \{0, 1, 4, 7\} \mapsto S_3 = \{0, 1, 2, 3\}$ . The corresponding permutation of amplitudes is then implemented using the gate constructions described in Section 6:

$$\begin{array}{ll} 000 \rightarrow 000 & \rightarrow 000 \\ 001 \rightarrow 001 & \rightarrow 001 \\ 100 \rightarrow \text{SWAP}_{(|j_2\rangle, |j_1\rangle)} & \rightarrow 010 \\ 111 \rightarrow X_{|j_2\rangle} C(1_{|j_1\rangle}) C(1_{|j_0\rangle}) & \rightarrow 011 \end{array}$$

where  $\text{SWAP}_{(|j_2\rangle, |j_1\rangle)}$  denotes SWAP gate applied between qubits  $|j_2\rangle$  and  $|j_1\rangle$ ,  $C(1_{|j_1\rangle})$  denotes a control on qubit  $|j_1\rangle$  with control value 1, and  $X_{|j_2\rangle}$  denotes a NOT gate applied on qubit  $|j_2\rangle$ . A controlled-SWAP gate can also be used to swap only two amplitudes according to the permutation requirements. The combined deletion can be performed by

$$D_a^{\{0,1,4,7\}} = C_{(\vec{a})} X_{|\text{del}\rangle} C_{(0XX)}, \quad (19)$$

where  $C_{(\vec{a})}$  denotes control on data qubits ( $|\text{data}\rangle$ ) and  $C_{(0XX)}$  denotes control on the matrix qubit  $|j_2\rangle$  alone. After the deletion, the rows can be arranged to their original order. The circuit for this example is shown in Fig. 5e.

Furthermore, a many-to-many mapping is also possible, where more than one data item can be deleted in multiple rows, provided that the set of rows to be deleted is common for all data items.

### 7.3. Insert

We have seen how to delete a data item in multiple rows. However, if the task is to insert a data item into one or a few rows, performing deletion

on all other rows would require many MCX gates. Therefore, in this section, we introduce the insert operator, as illustrated in Example 7.5.

**Example 7.5.** *The data items  $\{a, b\}$  are to be inserted in different rows  $\{r_a, r_b\}$ , respectively, corresponding to a one-to-one mapping.*

*Solution:* To insert a single data item  $a$  in row  $r_a$ , we define

$$I_a^{r_a} = D_a^{r_{\text{all}}} D_a^{r_a}, \quad (20)$$

where  $r_{\text{all}}$  means all rows. Since the proposed block encoding method places each data item in all rows Eq. (9), we first delete the data item from all rows and then apply deletion on the desired row  $r_a$ . This effectively inverts the deletion on the desired row, resulting in the insertion of the data item in that row alone.

To insert a set of data items  $\{a, b\}$  into rows  $\{r_a, r_b\}$ , we formulate

$$I_a^{r_a} I_b^{r_b} = D_a^{r_{\text{all}}} D_a^{r_a} D_b^{r_{\text{all}}} D_b^{r_b} = D_{\{a,b\}}^{r_{\text{all}}} D_a^{r_a} D_b^{r_b}. \quad (21)$$

The circuit representation for this task is shown in Fig. 5f, where  $A_{\text{PERMUTE}_R}$  (represented as  $P_R$ ) is included for right-ended permutation of amplitudes. Note that deletion in all rows corresponds to a composition of MCX gates as in Section 4, where  $P = n$ , resulting in no control on the matrix qubits.

## 8. Complete Circuit

In this section, we present the complete circuit for block encoding of sparse matrices, including the optimized index mapping oracle (see Section 7). For clarity, the procedure can be summarized as follows:

1. Given a sparse matrix, construct the data vector Eq. (4), where each data item corresponds to a unique diagonal element (for a fixed diagonal offset).
2. Obtain the state preparation oracle for the PREP and UNPREP operators Eqs. (7) and (8) (see Section 3.1).
3. Tabulate the required shift, delete, and insert operations for each data item.
4. Identify common operators using the optimized index mapping oracle Section 7.
5. Check for control states in  $S_2$ , and generate  $S_3$  if necessary Section 5.

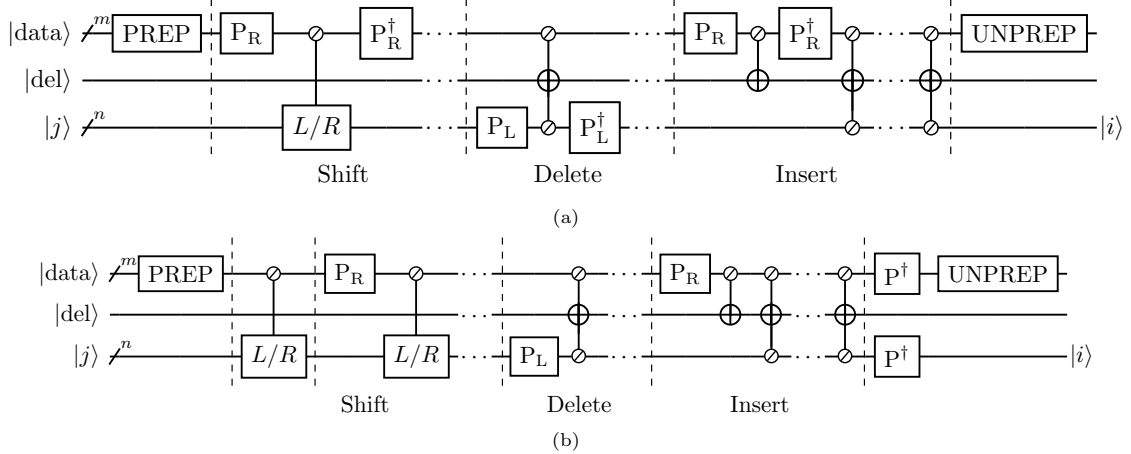


Figure 6: a Circuit representation for block encoding with coherent permutation. The circuit is initialized with  $m$   $|\text{data}\rangle$ , one  $|\text{del}\rangle$  and  $n$  matrix ( $|j\rangle$ ) qubits. It includes the PREP and UNPREP operators from the state preparation oracle (see Section 3.1). The combined shift, delete, and insert operators Figs. 5a, 5d and 5f are incorporated along with the corresponding A\_PERMUTE (represented as  $P$ ) operators for permutation. The dots indicate repeating structures. b Circuit representation for further simplification, where amplitude order must be tracked and restored by applying the inverse permutation operator ( $P^\dagger$ ) at the end.

6. Determine the coherent permutation gates for amplitude reordering, if required Section 6.
7. Apply all operations within a single circuit to obtain the scaled matrix block encoded as in Eq. (1), and multiply by the subnormalization factor  $\alpha$  to recover the original matrix.

An overview of the circuit architecture for block encoding is shown in Fig. 6a. In this design, the amplitudes are permuted back after every combined operation, ensuring that the order of amplitudes remains consistent throughout the circuit. Let amplitude-permuting operator A\_PERMUTE consists of  $n$  MCX gates. Then,

$$\begin{aligned} \text{A\_PERMUTE} &= \prod_{i=0}^{n-1} \text{MCX}_i, \\ \text{A\_PERMUTE}^\dagger &= \prod_{i=n-1}^0 \text{MCX}_i, \end{aligned} \quad (22)$$

where the inverse operation uses the same MCX gates applied in reverse order.

A potential optimization is illustrated in Fig. 6b. Here, the state preparation oracle initializes the amplitudes in an order already suited to the first combined shift operator. Then the amplitudes are permuted only once before each combined operation, and not reordered back to their original configuration at intermediate steps. This means the order of amplitudes evolve after each A\_PERMUTE

application, and finally they are restored by applying  $\text{A\_PERMUTE}^\dagger$  at the end of the circuit. If  $\text{A\_PERMUTE}^\dagger$  is implemented strictly as in Eq. (22), the construction closely resembles Fig. 6a.

A promising research direction is to explore permutation of amplitudes in arbitrary order to avoid strict reversal using the techniques discussed in Section 6. That said, this requires careful bookkeeping of the evolving amplitude order, and permuting arbitrary orders may become increasingly costly as the number of permutations grows.

## 9. Applications

In this section, we present two examples of sparse matrix block encoding: a complex tridiagonal matrix and a structured real matrix.

### 9.1. Complex Tridiagonal Matrix

Consider a complex tridiagonal matrix  $A \in \mathbb{C}^{2^n \times 2^n}$  of the form,

$$A = \begin{bmatrix} z_2 & z_3 & & & \\ z_1 & z_2 & z_3 & & \\ \ddots & \ddots & \ddots & \ddots & \\ & z_1 & z_2 & z_3 & \\ & & z_1 & z_2 & \end{bmatrix}, \quad (23)$$

where  $z_1 = a + bi$ ,  $z_2 = c + di$ ,  $z_3 = e + fi$  and  $\{a, b, c, d, e, f\} \in \mathbb{R}$ . The corresponding data vector

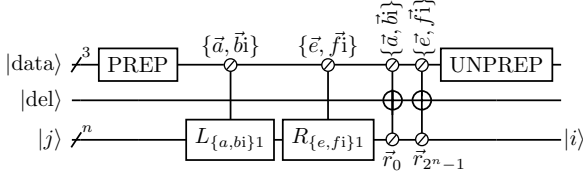


Figure 7: Circuit representation for block encoding complex tridiagonal matrix Eq. (23). The control states are represented by binary representation as in Fig. 3.

is

$$A_{\text{data}} = [|a|, |b|, |c|, |d|, |e|, |f|]^T \text{ (refer Eq. (4))}$$

with sign vector

$$\begin{aligned} \text{sgn}(A_{\text{data}}) = & [\text{sgn}(a), \text{sgn}(b)i, \text{sgn}(c), \text{sgn}(d)i, \\ & \text{sgn}(e), \text{sgn}(f)i]^T \text{ (refer Eq. (5)).} \end{aligned}$$

State preparation requires  $\lceil \log_2 6 \rceil = 3$  data qubits (refer Theorem 1), where the state can be padded with zeros. For block encoding, the data items  $\{a, bi\}$  must be shifted left by one column and deleted in row  $\vec{r}_0$  as in Eq. (10). If required, amplitudes can be permuted for nearest-neighbor MCX gate connectivity. Similarly, the data items  $\{e, fi\}$  must be shifted right by one column and deleted in row  $\vec{r}_{2^n-1}$  as in Eq. (11).

The circuit representation of this construction is shown in Fig. 7 and provides a practical gate-level realization that can be directly employed within quantum algorithms. Note that zeros in the state vector can also be leveraged for combined shifting (see Example 7.3), thereby reducing the control complexity of the MCX gates.

## 9.2. Structured Real Matrix

Consider a sparse real matrix  $A = \mathbb{R}^{32 \times 32}$  with the structure shown in Fig. 8a. Following the block-encoding procedure outlined in Section 8, the corresponding data vector is  $A_{\text{data}} = [a_i]^T$ ,  $a_i \in \mathbb{R}$ ,  $i \in [0, 13]$ . The number of data qubits required for block encoding is  $\lceil \text{Dim}(A_{\text{data}}) \rceil = 4$ , where the state vector is padded with zeros for state preparation.

The block-encoding operations (shift, delete, insert) are summarized in Table 1 (refer also to Section 7). Note that two distinct values  $(a_2, a_3)$ , occur on the main diagonal. Within the block-encoding framework, these appear as the combined diagonal value  $a_2 + a_3$  (see Eq. (9)). To address this issue, we outline three possible encoding strategies with

an objective to reduce MCX gates and subnormalization factor:

1. Block Encode:  $a_2, a_3$ ,  
Delete operations:  $a_2 : D_{a_2}^{\{5-31\}}$ ,  $a_3 : D_{a_3}^{\{0-4\}}$ ,  
Subnormalization factor within  $\alpha$ :  $|a_2| + |a_3|$ .
2. Block Encode:  $\tilde{a}_2 = a_3 - a_2$ ,  $\tilde{a}_3 = a_2$ ,  
Delete operations:  $\tilde{a}_2 : D_{\tilde{a}_2}^{\{0-4\}}$ ,  $\tilde{a}_3 : \text{Nothing}$ ,  
Subnormalization factor within  $\alpha$ :  $|\tilde{a}_2| + |\tilde{a}_3|$ ,  
This is advantageous when  $|a_3 - a_2| < |a_3|$ .
3. Block Encode  $\tilde{a}_2 = a_3$ ,  $\tilde{a}_3 = a_2 - a_3$ ,  
Delete operations:  $\tilde{a}_2 : \text{Nothing}$ ,  $\tilde{a}_3 : D_{\tilde{a}_3}^{\{5-31\}}$ ,  
Subnormalization factor within  $\alpha$ :  $|\tilde{a}_2| + |\tilde{a}_3|$ ,  
This is advantageous when  $|a_2 - a_3| < |a_2|$ .

For demonstration, we choose the second approach as illustrated in Table 1.

For non-repeating diagonal entries of  $A_{ij}$ , the shift operations are defined as  $R_{\text{shift}} = i - j$ ,  $L_{\text{shift}} = j - i$ . For values  $[a_6, \dots, a_{13}]$  in Table 1, all are encoded via left shifts, since they can be combined with other data items. However, right shifts may also be employed depending on the matrix structure. Next, we determine the common shift operators, shown in Table 2, while the delete and insert operations are retained as in Table 1.

Block encoding operations
$a_0, L_5 = L_1 L_4, D_{a_0}^{\{0-9\}}$
$a_1, L_1, D_{a_1}^{\{0,5,10,15,20,25,30,31\}}$
$\tilde{a}_2 = a_3 - a_2, D_{\tilde{a}_2}^{\{0-4\}}$
$\tilde{a}_3 = a_2$
$a_4, R_1, D_{a_4}^{\{4,9,14,19,24,29,30,31\}}$
$a_5, R_5 = R_1 R_4, D_{a_5}^{\{0-4,27-31\}}$
$a_6, L_6 = L_2 L_4, I_{a_6}^6$
$a_7, L_9 = L_1 L_8, I_{a_7}^{10}$
$a_8, L_{11} = L_1 L_2 L_8, I_{a_8}^{12}$
$a_9, L_{14} = L_2 L_4 L_8, I_{a_9}^{16}$
$a_{10}, L_{16}, I_{a_{10}}^{18}$
$a_{11}, L_{19} = L_1 L_2 L_{16}, I_{a_{11}}^{22}$
$a_{12}, L_{21} = L_1 L_4 L_{16}, I_{a_{12}}^{24}$
$a_{13}, L_{24} = L_8 L_{16}, I_{a_{13}}^{28}$
$a_{14} = 0$
$a_{15} = 0$

Table 1: Block encoding operations for Fig. 8a, with data values  $[a_i]_{i=0}^{15}$ . Here,  $\tilde{a}_2, \tilde{a}_3$  denote modified values of  $a_2, a_3$  in the data vector. Shift operations are indicated as left  $L_{\text{shift}}$  or right  $R_{\text{shift}}$ . Deletion operations are denoted by  $D_{a_i}^{r_{a_i}}$ , where  $r_{a_i}$  is the target row for deleting  $a_i$ . Similarly, insert operations are represented as  $I_{a_i}^{r_{a_i}}$ .

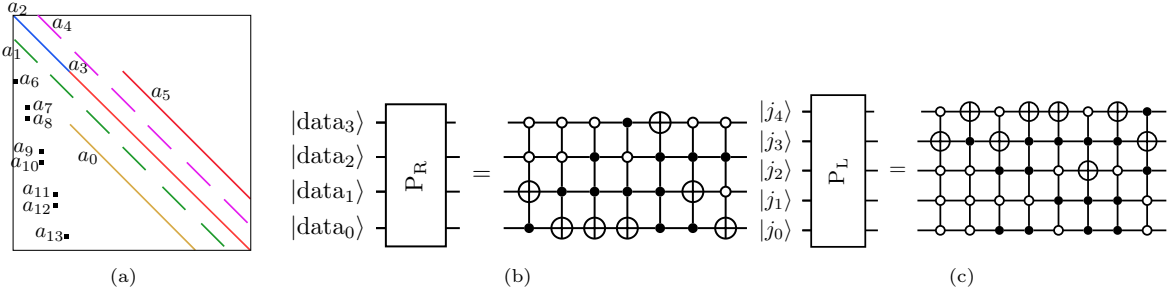


Figure 8: a Visual representation of the example sparse matrix structure (see Section 9.2). The data items are denoted by  $[a_i]_{i=0}^{13}$ . Continuous lines of the same color indicate the repeating pattern of a data item ( $a_i$ ) along a diagonal with a fixed offset, while black square dots denote single, non-repeating data items. b Coherent permutation on the data qubits Eq. (24). c Coherent permutation on the matrix qubits Eq. (25).

Common shift operators	
$L_1$	$a_0, a_1, a_7, a_8, a_{11}, a_{12}, a_{14}, a_{15}$
$L_2$	$a_6, a_8, a_9, a_{11}$
$L_4$	$a_0, a_6, a_9, a_{12}$
$L_8$	$a_7, a_8, a_9, a_{13}$
$L_{16}$	$a_{10}, a_{11}, a_{12}, a_{13}$
$R_1$	$a_4, a_5$
$R_4$	$a_5$

Table 2: Common shift operations of the data items Table 1. Note that the  $L_1$  shift involves six data items; however, as illustrated in Example 7.3, the zeros in  $a_{14}$  and  $a_{15}$  can be exploited to extend this to eight shifts.

The next step is to determine whether amplitude permutation is required. For demonstration purposes, we consider the shift  $L_1$  in Table 2 and the deletion  $D_{a_1}$  in Table 1. For  $L_1$ , the control states  $S_2$  corresponding to the data items  $[a_0, a_1, a_7, a_8, a_{11}, a_{12}, a_{14}, a_{15}]$  do not satisfy the constraint in Theorem 2. Therefore, we apply the permutation operator  $A_{\text{PERMUTE}}_R$  as shown in Fig. 5a. Following Theorem 3, the mapping  $\phi : S_2 \mapsto S_3$  is obtained using the linear sum assignment algorithm [39]. Finally, the gates are generated to permute  $(S_2, S_3)$  according to Definition 6.2, resulting in the following transformation:

$$\begin{aligned}
 a_0 & 0000 \\
 a_1 & 0001 \rightarrow 0011 \rightarrow 0010 \\
 a_7 & 0111 \rightarrow 0110 \\
 a_8 & 1000 \\
 a_{11} & 1011 \rightarrow 1010 \\
 a_{12} & 1100 \\
 a_{14} & 1110 \\
 a_{15} & 1111 \rightarrow 0111 \rightarrow 0101 \rightarrow 0100
 \end{aligned} \quad . \quad (24)$$

The MCX gates implementing the mapping in Eq. (24) (see Definition 6.2) correspond to the operator  $A_{\text{PERMUTE}}_R$ , as illustrated in Fig. 8b. Note that, alternatively, one may employ multi-controlled SWAP gates for specific cases such as  $a_1$  (e.g.,  $0001 \mapsto 0010$ ), or consider multi-swapping strategies as discussed in Theorem 4.

Considering the combined delete  $D_{a_1}$ , the control states  $S_2$  corresponding to rows  $[0, 5, 10, 15, 20, 25, 30, 31]$  do not satisfy the constraint in Theorem 2. Therefore, we implement the operator  $A_{\text{PERMUTE}}_L$ , as shown in Fig. 5d. Following the same protocol as for the previous case, we obtain the mapping  $\phi : S_2 \mapsto S_3$ , leading to the following transformation:

$$\begin{aligned}
 0 & 00000 \rightarrow 01000 \rightarrow 11000 \\
 5 & 00101 \rightarrow 01101 \rightarrow 11101 \\
 10 & 01010 \rightarrow 11010 \\
 15 & 01111 \rightarrow 01011 \rightarrow 11011 \\
 20 & 10100 \rightarrow 11100 \\
 25 & 11001 \\
 30 & 11110 \\
 31 & 11111
 \end{aligned} \quad . \quad (25)$$

The MCX gates corresponding to the mapping in Eq. (25) (see Definition 6.2) are implemented through  $A_{\text{PERMUTE}}_L$ , as illustrated in Fig. 8c. The complete circuit for block encoding the matrix Fig. 8a is obtained by combining the shift, delete, insert, and permutation operators, as shown in Fig. 6. This circuit provides a practical gate-level realization that can be directly employed within quantum algorithms.

## 10. Discussion

In this work, we have significantly extended the understanding of block encoding of sparse matrices by providing detailed gate-level implementations together with novel strategies that enable practical access to quantum circuits for arbitrary sparse matrices. In particular, we offered an intuitive explanation of the existing PREP/UNPREP-based block encoding framework and generalized it to support complex matrices.

A key observation of our analysis is that the subnormalization factor  $\alpha = \sum_{p=0}^{s-1} |A_p| > \|A\|_2$ , is greater than spectral norm. Whether there exists a block encoding scheme where the subnormalization factor matches the spectral norm remains an open fundamental question in the field, with profound implications for the efficiency of QSVD-based algorithms. Likewise, our framework provides a new perspective that could enable more systematic estimation of quantum resource requirements [9, 10].

On the circuit-design side, we demonstrated how natural compositions of MCX gates emerge in block encoding, and how these can be compressed into single MCX operations under suitable constraints (Section 4), directly reducing depth and cost. We then introduced a novel connection between amplitude reordering and combinatorial optimization, formulating the placement of MCX control qubits as an optimization problem on the hardware connectivity graph. This approach minimizes the number of permutations while respecting nearest-neighbor constraints, bridging quantum circuit compilation and classical optimization theory.

Our proposed coherent permutation operators provide an additional advantage: they are fully unitary, preserving superposition and entanglement during amplitude reordering. Unlike conventional two-amplitude swaps, our method extends to multi-amplitude permutations (Theorem 4), laying the groundwork for systematic reduction of MCX gates into two-qubit primitives better suited for current hardware. This perspective opens a new research direction where permutation design itself could become a tool for circuit optimization.

To bridge theory and hardware, we demonstrated an optimized index mapping oracle that naturally yields nearest-neighbor MCX gates, addressing the connectivity constraints of superconducting qubit platforms. By integrating all components, we constructed the complete circuit for block encoding of sparse matrices Fig. 6 and discussed how future ar-

chitectures could exploit low-complexity permutation layers to further enhance scalability.

Finally we validated our framework by implementing it on two respective cases: a complex tridiagonal matrix and a structured real matrix, demonstrating that the entire pipeline from theory to circuit operates seamlessly. The resulting circuits are immediately applicable to high-impact quantum algorithms such as QSVD, HHL, and Hamiltonian simulation [40], thereby extending the reach of block encoding into practical algorithm design and realistic hardware execution.

## Acknowledgements

This research was funded through the European Union’s Horizon Programme (HORIZONCL4-2021-DIGITALEMERGING-02-10), Grant Agreement 101080085 (QCFD).

## References

- [1] A. Gilyén, Y. Su, G. H. Low, N. Wiebe, Quantum singular value transformation and beyond: exponential improvements for quantum matrix arithmetics, in: Proceedings of the 51st annual ACM SIGACT symposium on theory of computing, 2019, pp. 193–204.
- [2] A. W. Harrow, A. Hassidim, S. Lloyd, Quantum algorithm for linear systems of equations, *Physical review letters* 103 (15) (2009) 150502.
- [3] D. W. Berry, A. M. Childs, R. Cleve, R. Kothari, R. D. Somma, Simulating hamiltonian dynamics with a truncated taylor series, *Physical review letters* 114 (9) (2015) 090502.
- [4] A. M. Childs, R. Kothari, R. D. Somma, Quantum algorithm for systems of linear equations with exponentially improved dependence on precision, *SIAM Journal on Computing* 46 (6) (2017) 1920–1950.
- [5] A. M. Childs, N. Wiebe, Hamiltonian simulation using linear combinations of unitary operations, *arXiv preprint arXiv:1202.5822* (2012).
- [6] F. G. Brandao, K. M. Svore, Quantum speed-ups for solving semidefinite programs, in: 2017 IEEE 58th Annual Symposium on Foundations of Computer Science (FOCS), IEEE, 2017, pp. 415–426.

[7] J. Van Apeldoorn, A. Gilyén, S. Gribling, R. de Wolf, Quantum sdp-solvers: Better upper and lower bounds, in: 2017 IEEE 58th Annual Symposium on Foundations of Computer Science (FOCS), IEEE, 2017, pp. 403–414.

[8] R. Babbush, C. Gidney, D. W. Berry, N. Wiebe, J. McClean, A. Paler, A. Fowler, H. Neven, Encoding electronic spectra in quantum circuits with linear t complexity, *Physical Review X* 8 (4) (2018) 041015.

[9] B. D. Clader, A. M. Dalzell, N. Stamatopoulos, G. Salton, M. Berta, W. J. Zeng, Quantum resources required to block-encode a matrix of classical data, *IEEE Transactions on Quantum Engineering* 3 (2023) 1–23.

[10] S. Chakraborty, A. Gilyén, S. Jeffery, The power of block-encoded matrix powers: improved regression techniques via faster hamiltonian simulation, *arXiv preprint arXiv:1804.01973* (2018).

[11] D. Camps, R. Van Beeumen, Fable: Fast approximate quantum circuits for block-encodings, in: 2022 IEEE International Conference on Quantum Computing and Engineering (QCE), IEEE, 2022, pp. 104–113.

[12] P. Kuklinski, B. Rempfer, S-fable and ls-fable: Fast approximate block-encoding algorithms for unstructured sparse matrices, *arXiv preprint arXiv:2401.04234* (2024).

[13] Z. Li, X.-M. Zhang, C. Yang, G. Zhang, Binary tree block encoding of classical matrix, *arXiv preprint arXiv:2504.05624* (2025).

[14] D. Camps, L. Lin, R. Van Beeumen, C. Yang, Explicit quantum circuits for block encodings of certain sparse matrices, *SIAM Journal on Matrix Analysis and Applications* 45 (1) (2024) 801–827.

[15] C. Sünderhauf, E. Campbell, J. Camps, Block-encoding structured matrices for data input in quantum computing, *Quantum* 8 (2024) 1226.

[16] C. Yang, H. Yao, Z. Li, Z. Fan, G. Zhang, J. Liu, Block encoding of sparse structured matrices coming from ocean acoustics in quantum computing, *arXiv preprint arXiv:2405.18007* (2024).

[17] V. V. Shende, S. S. Bullock, I. L. Markov, Synthesis of quantum logic circuits, in: Proceedings of the 2005 Asia and South Pacific Design Automation Conference, 2005, pp. 272–275.

[18] M. Amy, D. Maslov, M. Mosca, M. Roetteler, A meet-in-the-middle algorithm for fast synthesis of depth-optimal quantum circuits, *IEEE Transactions on Computer-Aided Design of Integrated Circuits and Systems* 32 (6) (2013) 818–830.

[19] A. Cowtan, S. Dilkes, R. Duncan, A. Krajenbrink, W. Simmons, S. Sivarajah, On the qubit routing problem, *arXiv preprint arXiv:1902.08091* (2019).

[20] P. Murali, J. M. Baker, A. Javadi-Abhari, F. T. Chong, M. Martonosi, Noise-adaptive compiler mappings for noisy intermediate-scale quantum computers, in: Proceedings of the twenty-fourth international conference on architectural support for programming languages and operating systems, 2019, pp. 1015–1029.

[21] A. Barenco, C. H. Bennett, R. Cleve, D. P. DiVincenzo, N. Margolus, P. Shor, T. Sleator, J. A. Smolin, H. Weinfurter, Elementary gates for quantum computation, *Physical review A* 52 (5) (1995) 3457.

[22] D. M. Miller, D. Maslov, G. W. Dueck, A transformation based algorithm for reversible logic synthesis, in: Proceedings of the 40th annual Design Automation Conference, 2003, pp. 318–323.

[23] D. Maslov, Advantages of using relative-phase toffoli gates with an application to multiple control toffoli optimization, *Physical Review A* 93 (2) (2016) 022311.

[24] N. M. Linke, D. Maslov, M. Roetteler, S. Debnath, C. Figgatt, K. A. Landsman, K. Wright, C. Monroe, Experimental comparison of two quantum computing architectures, *Proceedings of the National Academy of Sciences* 114 (13) (2017) 3305–3310.

[25] R. Beals, S. Brierley, O. Gray, A. W. Harrow, S. Kutin, N. Linden, D. Shepherd, M. Stather, Efficient distributed quantum computing, *Proceedings of the Royal Society A: Mathematical, Physical and Engineering Sciences* 469 (2153) (2013) 20120686.

[26] S. A. Kutin, D. P. Moulton, L. M. Smithline, Computation at a distance, arXiv preprint quant-ph/0701194 (2007).

[27] R. W. Hamming, Error detecting and error correcting codes, *The Bell system technical journal* 29 (2) (1950) 147–160.

[28] J. Li, S. Lin, K. Yu, G. Guo, Quantum k-nearest neighbor classification algorithm based on hamming distance, *Quantum Information Processing* 21 (1) (2022) 18.

[29] M. Mottonen, J. J. Vartiainen, V. Bergholm, M. M. Salomaa, Transformation of quantum states using uniformly controlled rotations, arXiv preprint quant-ph/0407010 (2004).

[30] M. Möttönen, J. J. Vartiainen, V. Bergholm, M. M. Salomaa, Quantum circuits for general multiqubit gates, *Physical review letters* 93 (13) (2004) 130502.

[31] R. Iten, R. Colbeck, I. Kukuljan, J. Home, M. Christandl, Quantum circuits for isometries, *Physical Review A* 93 (3) (2016) 032318.

[32] X.-M. Zhang, T. Li, X. Yuan, Quantum state preparation with optimal circuit depth: Implementations and applications, *Physical Review Letters* 129 (23) (2022) 230504.

[33] H. W. Kuhn, The hungarian method for the assignment problem, *Naval research logistics quarterly* 2 (1-2) (1955) 83–97.

[34] J. Munkres, Algorithms for the assignment and transportation problems, *Journal of the society for industrial and applied mathematics* 5 (1) (1957) 32–38.

[35] R. Burkard, M. Dell’Amico, S. Martello, Assignment problems: revised reprint, SIAM, 2012.

[36] L. A. Wolsey, Integer programming, John Wiley & Sons, 2020.

[37] A. Schrijver, et al., Combinatorial optimization: polyhedra and efficiency, Vol. 24, Springer, 2003.

[38] B. Korte, J. Vygen, Combinatorial optimization: theory and algorithms, Springer, 2008.

[39] D. F. Crouse, On implementing 2d rectangular assignment algorithms, *IEEE Transactions on Aerospace and Electronic Systems* 52 (4) (2016) 1679–1696.

[40] J. M. Martyn, Z. M. Rossi, A. K. Tan, I. L. Chuang, Grand unification of quantum algorithms, *PRX quantum* 2 (4) (2021) 040203.